Journal of Systems Engineering and Electronics
Vol. PP, No. 99, May 2023, pp.1 – 9

An angular blinking jamming method based on electronically controlled corner reflectors

GAN Lin, WU Zehao, WANG Xuesong, and LI Jianbing*

State Key Laboratory of Complex Electromagnetic Environmental Effects on Electronics and Information System, National University of Defense Technology, Changsha 410073, China

Abstract: Passive jamming is believed to have very good potential in countermeasure community. In this paper, a passive angular blinking jamming method based on electronically controlled corner reflectors is proposed. The amplitude of the incident wave can be modulated by switching the corner reflector between the penetration state and the reflection state, and the ensemble of multiple corner reflectors with towing rope can result in complex angle decoying effects. Dependency of the decoying effect on corner reflectors' radar cross section and positions are analyzed and simulated. Results show that the angle measured by a monopulse radar can be significantly interfered by this method while the automatic tracking is employed.

Keywords: monopulse radar, angular blinking jamming, corner reflector, amplitude-comparison angle measurement, metasurface.

DOI: 10.23919/JSEE.2023.000068

1. Introduction

Monopulse radar is a kind of precise angle measuring radar, whose antennas can form multiple identical beams to obtain the azimuth and elevation angles during one single pulse [1,2]. Compared with the conical scanning radar, the monopulse radar has the advantages of high angle measurement accuracy and good anti-jamming ability. It has been widely used in target identification, tracking, navigation and other fields, and the corresponding countermeasure method is of great significance in self-defense of high-value targets such as fighters.

A good variety of angle deception jamming techniques have been developed to interfere the monopulse radar, such as terrain bounce jamming [3,4], blinking jamming [5,6], towed decoys [7], and cross-eye jamming [8−10]. The key components in these methods are the active jammers, which are generally expensive and less flexible to different countermeasure scenarios. Passive jamming equipment such as chaff and corner reflector is much cheaper, but their electromagnetic scattering characteristics are fixed and their ability to modulate the incident wave is quite limited. Great efforts should be made to develop new passive jamming method with better interference effects.

Over the past several years, increasing attention has been paid to metamaterial which can precisely control the amplitude, phase, polarization, and other parameters of the electromagnetic wave [11,12]. If the metasurface can be combined with corner reflectors with strong scattering capabilities, electromagnetic structures with high energy and strong modulation capabilities can be formed. Currently, this combination has been initially studied in the communication field, mainly for selecting frequency bands [13], reconstructing beams [14−16], and improving antenna gains [17−20]. In the field of electronic countermeasures, metamaterials are mainly used to change the inherent properties of corner reflectors to make up for their deficiencies in passive interference applications. Zhu et al. combined metamaterial absorbers with dihedral and trihedral corner reflectors, so that they could effectively counter the X-band frequency agile radar [21,22]. Zhang et al. [23] and Lei et al. [24] effectively improved the backscattering ability of the corner reflector by metamaterials. Zhang et al. proposed a dihedral corner reflector based on the Salisbury screen, which has a remarkable effect in changing the polarization characteristic and other features [25]. It is foreseeable that electronically controlled corner reflectors also have great potential in the tracking radar jamming field. Aiming at the angle measurement interference of a monopulse radar, the interference effects and influencing factors of a towed

Manuscript received July 04, 2022.
*Corresponding author.
This work was supported by the Equipment Pre-research Project (GK202002A020068).

electronically controlled corner reflector are studied in this paper.

This paper is organized as follows: Section 2 introduces the principle of angular blinking jamming and quantitatively analyzes the influence of some key parameters on the angle measurement. Section 3 validates the decoying effect under different radar cross section (RCS) modulation signals and synergy patterns of the corner reflectors in the automatic angle tracking process. Conclusions are drawn in Section 4.

2. Blinking jamming of electronically controlled corner reflectors based on amplitude-comparison angle measurement

The amplitude-comparison measurement is a classical and widely-used method for precise angular information measurement of the target by comparing the amplitude of the radar echoes of multiple beams in one single pulse. We first analyze the principle when electronically controlled corner reflectors are introduced in the angle measurement scenario.

2.1 Fundamentals of blinking jamming

Taking the elevation direction as an example, the angle between the center axis of each radar beam and the equisignal axis is θ_k, and the radiation pattern of each radar antenna is $F(\theta)$. The elevation angle of the target [26] can be calculated by

$$\hat{\theta} = \frac{\Delta}{\Sigma} \cdot \left[\frac{F'(\theta_k)}{F(\theta_k)} \right]^{-1} \tag{1}$$

where Δ and Σ are the difference and sum of the received signals, respectively. In order to protect targets such as the fighter, we have to interfere this angle measurement process. Towered decoy is a widely-used method to complete this task, but it greatly depends on the towed active jammers. It is of great importance if we can develop a passive jamming method with complex interference effects. This can be realized by towing multiple electronically controlled corner reflectors and modulating their electromagnetic characteristics with complex schemes. In addition, the advantages of low cost and simple fabrication make it possible to deploy multiple corner reflectors in one angle resolution cell.

As shown in Fig. 1, there are multiple scattering points in one angle resolution cell when the aircraft drags several corner reflectors. The amplitude and phase of the radar echo change continuously with the movement of all objects, resulting in the deviation of the apparent angle. If RCSs of the corner reflectors are electronically modulated, complex angular glint effects can be obtained.

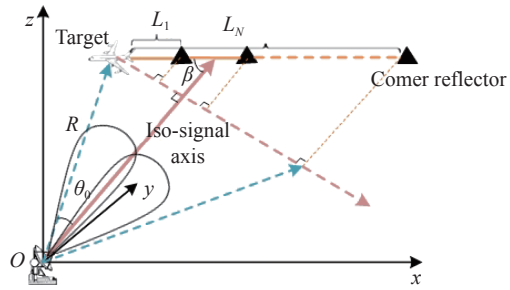

Fig. 1 Jamming scenario

Assuming that the RCS of the target is fixed, the sum and difference signals received by the radar are respectively

$$\Sigma = \sigma_0 \mathrm{e}^{\mathrm{j}\varphi_0} [F(\theta_0 + \theta_k) + F(\theta_0 - \theta_k)] + \sum_{i=1}^{N} \sigma_i(t) \mathrm{e}^{\mathrm{j}\varphi_i} [F(\theta_i + \theta_k) + F(\theta_i - \theta_k)], \tag{2}$$

$$\Delta = \sigma_0 \mathrm{e}^{\mathrm{j}\varphi_0} [F(\theta_0 + \theta_k) - F(\theta_0 - \theta_k)] + \sum_{i=1}^{N} \sigma_i(t) \mathrm{e}^{\mathrm{j}\varphi_i} [F(\theta_i + \theta_k) - F(\theta_i - \theta_k)], \tag{3}$$

where σ_0 is the RCS of the target to be protected, φ_0 and φ_i are the echo phases of the target and the ith corner reflector respectively, θ_0 is the angle between the target and the equisignal axis, θ_i is the angle between the ith corner reflector and the equisignal axis, L_i is the distance between the ith corner reflector and the target, N is the number of corner reflectors, and $\sigma_i(t)$ is the time-domain RCS modulated signal for the ith corner reflector which can have rapid amplitude change above 10 dB. Substituting (2) and (3) into (1), the measured angle $\hat{\theta}$ can be obtained as

$$\hat{\theta} = k_0 \left\{ \sigma_0 \mathrm{e}^{\mathrm{j}\varphi_0} [F(\theta_0 + \theta_k) - F(\theta_0 - \theta_k)] + \sum_{i=1}^{N} \sigma_i(t) \mathrm{e}^{\mathrm{j}\varphi_i} [F(\theta_i + \theta_k) - F(\theta_i - \theta_k)] \right\} \cdot \left\{ \sigma_0 \mathrm{e}^{\mathrm{j}\varphi_0} [F(\theta_0 + \theta_k) + F(\theta_0 - \theta_k)] + \sum_{i=1}^{N} \sigma_i(t) \mathrm{e}^{\mathrm{j}\varphi_i} [F(\theta_i + \theta_k) + F(\theta_i - \theta_k)] \right\}^{-1} \tag{4}$$

where $k_0 = F(\theta_k)/F'(\theta_k)$. Assume that the radar observes the target laterally, as shown in Fig. 1, and the angle between the towing rope and the equisignal axis is β. The observing angle for a corner reflector θ_i can be approximated as follows:

$$\theta_i \approx \theta_0 + \frac{L_i \sin\beta}{R} \tag{5}$$

where R is the incident distance. Here it is assumed that the differences between the distances from the radar to corner reflectors are negligible. Then the measured angle

can be expressed as a multivariate function with independent variables θ_0, L_i, and $\sigma_i(t)$ by substituting (5) into (4)

$$\hat{\theta} = f(\theta_0, L_i, \sigma_i(t)) = k_0\left\{\sigma_0 \mathrm{e}^{\mathrm{j}\varphi_0}\left[F(\theta_0+\theta_k)-F(\theta_0-\theta_k)\right]+\sum_{i=1}^{N}\sigma_i(t)\mathrm{e}^{\mathrm{j}\varphi_i}\cdot\left[F\left(\theta_0+\frac{L_i\sin\beta}{R}+\theta_k\right)-F\left(\theta_0+\frac{L_i\sin\beta}{R}-\theta_k\right)\right]\right\}\cdot\left\{\sigma_0 \mathrm{e}^{\mathrm{j}\varphi_0}\left[F(\theta_0+\theta_k)+F(\theta_0-\theta_k)\right]+\sum_{i=1}^{N}\sigma_i(t)\mathrm{e}^{\mathrm{j}\varphi_i}\cdot\left[F\left(\theta_0+\frac{L_i\sin\beta}{R}+\theta_k\right)+F\left(\theta_0+\frac{L_i\sin\beta}{R}-\theta_k\right)\right]\right\}^{-1}. \quad (6)$$

Let $\boldsymbol{X}=[L_1, L_2, \cdots, L_N, \sigma_1, \sigma_2, \cdots, \sigma_N]$, then $f(\theta_0, \boldsymbol{X})$ can be approximated by its first-order Taylor expansion at $\boldsymbol{X}=\boldsymbol{0}$:

$$\hat{\theta} \approx f(\theta_0, \boldsymbol{X}=\boldsymbol{0}) + \left[\sum_{i=1}^{N}\left(L_i\frac{\partial}{\partial L_i}+\sigma_i(t)\frac{\partial}{\partial\sigma_i(t)}\right)\right] f(\theta_0, L_i, \sigma_i(t))|_{X=0}. \quad (7)$$

It can be seen that $f(\theta_0, \boldsymbol{X}=\boldsymbol{0})=\theta_0$, therefore the angle error caused by the towed corner reflectors can be obtained by

$$\theta_{\text{error}} = \hat{\theta}-\theta_0 = \left[\sum_{i=1}^{N}\left(L_i\frac{\partial}{\partial L_i}+\sigma_i(t)\frac{\partial}{\partial\sigma_i(t)}\right)\right]\cdot f(\theta_0, L_i, \sigma_i(t))|_{X=0}. \quad (8)$$

This paper focuses on the influence of L_i and $\sigma_i(t)$ on the measured angle $\hat{\theta}$, which can be obtained by calculating the partial derivative term in (8) numerically.

2.2 Quantitative analysis of influencing parameters

Assuming the target is located at (8 000 m, 4 000 m, 8 000 m), the RCS of the target is σ_0= 2 m^2, and the towing rope is parallel to the x-axis. Since the changing trends of the azimuth and elevation angle are the same, this section only lists the simulation results of the azimuth direction.

2.2.1 The towing rope length and the number of corner reflectors

Taking the double-point scenario as an example to show the influence. If the equisignal axis points to the target, then the factor $\partial f(\theta_0, L, \sigma_1)/\partial L$ which shows the relationship between the measurement error and the towing rope length is presented in Fig. 2. It can be seen that the error is almost linearly related to the towing rope length, and the slope increases along with the RCS of the corner reflector. This is physically reasonable, since both longer towing rope and stronger RCS will inevitably lead to bigger deviation of the apparent angle.

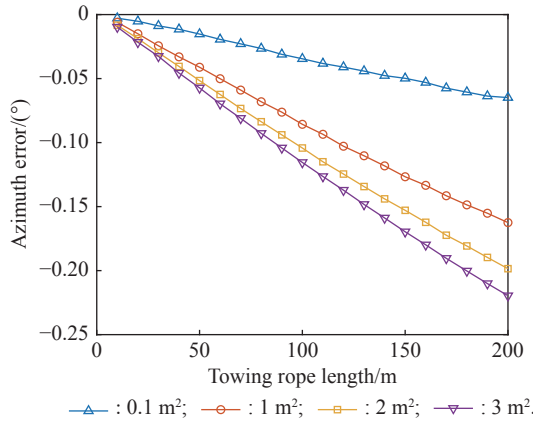

Fig. 2 Azimuth error under different L

Then we analyze the dependency of jamming effects on the number of corner reflectors. To ensure the jamming effectiveness, all the target and corner reflectors should be located in the same angle resolution cell by reasonably setting the towing rope length and the spacing between corner reflectors. The number N determines the distance L_i when they are equally spaced in the multi-point scenario. Assuming the total length is 200 m, and RCSs of all corner reflectors are the same. Fig. 3 presents the curves of the measurement error against the number of corner reflectors N, which show different trends under various σ_i. When σ_i is smaller than σ_0, the error increases along with N and the slope gradually decreases, while an opposite trend is observed when σ_i is larger than σ_0. Taking σ_i=3 m^2 as an example, the apparent angle is closer to the corner reflector when N = 1. As the number increases, the newly added corner reflectors are all on the left side of the current apparent center, making the apparent angle get closer to the target instead.

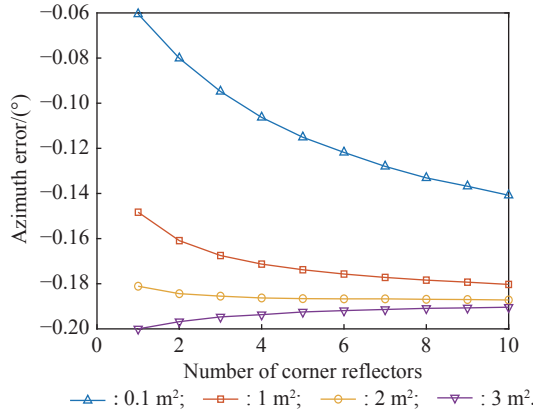

Fig. 3 Azimuth error under different N

2.2.2 RCS of the corner reflectors

Theoretically, larger RCS of corner reflectors can lead to stronger angular deviation, which can be confirmed by the variation curves in Fig. 4 of the measurement error along with σ_1 in the double-point scenario. However, as σ_1 increases, the slope of the curve gradually becomes smaller, which means that the efficiency of increasing σ_1 on improving the jamming effect gradually decreases. Therefore, the cost and effect of increasing RCS should be comprehensively considered to design an appropriate RCS value in practical applications. In addition, a larger distance can enhance the error-increasing effect.

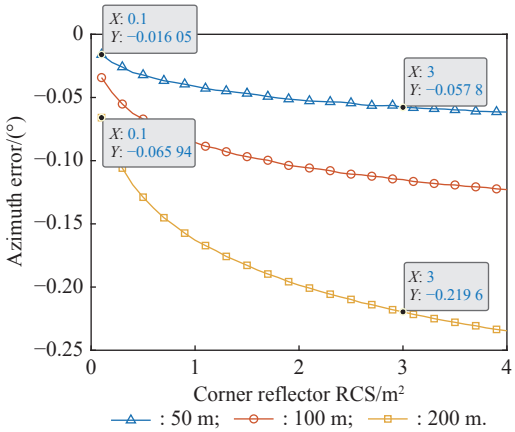

Fig. 4 Azimuth error under different σ_1

2.3 Implementation of jamming by electronically controlled corner reflectors

As shown in Fig. 5, an electronically controlled eight-quadrant corner reflector equipped with a miniaturized wave- penetrating active frequency-selective surface in [27] can be used to realize the interference scenarios. The RCS modulation depth of this surface can be maintained above 10 dB in the majority of directions. Therefore, it is feasible to apply this kind of corner reflector to the angle jamming field as a passive towed decoy. In practical applications, the size of the corner reflector can be designed according to specific needs. More wave-penetrating unit cells can be loaded if the size is larger, making it possible to increase the RCS modulation depth.

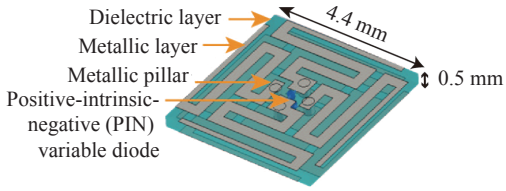

(a) Schematic diagram of the metasurface unit cell

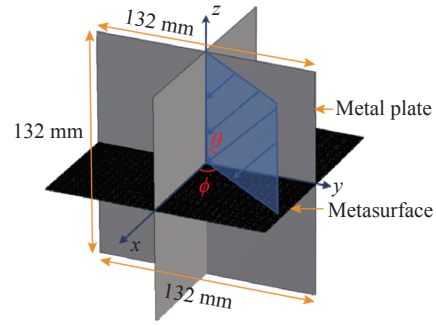

(b) Structure of the electronically controlled corner reflector

Fig. 5 Electronically controlled corner reflector based on the miniaturized wave-penetrating frequency-selective surface

In the scenario depicted in Fig. 1, the apparent angle can be constantly changed if the RCS of each corner reflector is electronically modulated, which can cause severe disturbance to the measured angle. The modulation mode can be summarized as an RCS modulation matrix shown in Fig. 6, where "1" represents the reflection state and "0" represents the penetration state. Two modulation dimensions are contained in the matrix: (i) the ith column represents the RCS time-domain modulation signal of the ith corner reflector. (ii) the relationship between adjacent columns represents the synergy pattern between the corner reflectors.

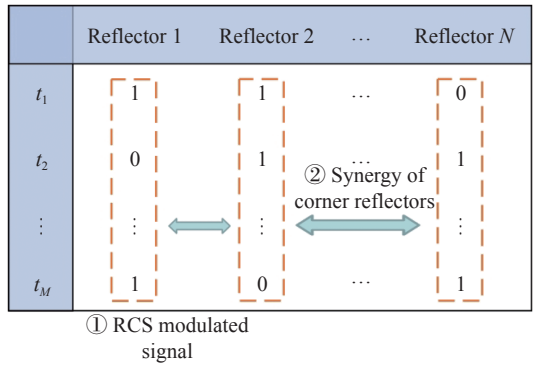

Fig. 6 RCS modulation matrix

Based on the above two dimensions, two RCS modulation signals containing the uniform intermittent and pseudo-random signals are designed in this paper, and the synergy patterns between corner reflectors are divided into three types, i.e., the synchronous change, the cyclic shift, and the random change. Sophisticated interference effects can be achieved through different combinations of modulation signals and synergy patterns.

Both the uniform intermittent and pseudo-random signal can be represented by the amplitude-encoded sequences:

$$\sigma_i(t)=\mathrm{rect}\left(\frac{t}{\tau_0}\right)\otimes\sum_{n=0}^{M-1}a_{i,n}(n+1)\delta(t-n\tau_0) \tag{9}$$

where $\otimes$ represents the convolution of signals, τ_0 represents the code width which is equal to the measuring sampling period, $a_{i,n}$ is the coding sequence only containing $\mathrm{RCS_{ref}}$ and $\mathrm{RCS_{pen}}$, the number of which is M_0 and $M-M_0$ respectively. $\mathrm{RCS_{ref}}$ and $\mathrm{RCS_{pen}}$ represent the RCS of the corner reflector in the reflection and penetration state. The duty ratio is defined as

$$\alpha=\frac{M_0}{M}. \tag{10}$$

$\mathrm{RCS_{ref}}$ and $\mathrm{RCS_{pen}}$ are set to 3 $\mathrm{m^2}$ and 0.1 $\mathrm{m^2}$ respectively. In order to evaluate the angle deception performance, the decoy ratio η is defined to represent the degree to which the apparent angle of the radar deviates from the real target. Expressions of the azimuth and elevation decoy ratio are

$$\eta_\varphi=\frac{\hat{\varphi}-\varphi_{\mathrm{target}}}{\varphi_{\mathrm{reflector\_last}}-\varphi_{\mathrm{target}}}, \tag{11}$$

$$\eta_\theta=\frac{\hat{\theta}-\theta_{\mathrm{target}}}{\theta_{\mathrm{reflector\_last}}-\theta_{\mathrm{target}}}, \tag{12}$$

where $\varphi_{\mathrm{reflector\_last}}$ and $\theta_{\mathrm{reflector\_last}}$ are the azimuth and elevation angle between the last corner reflector and the equisignal axis; $\varphi_{\mathrm{target}}$ and θ_{target} are those between the real target and the equisignal axis.

Predictably, when the RCSs of the corner reflectors are modulated by the uniform intermittent or pseudo-random signal, the apparent center of the radar will jump quickly between the near and far positions, showing periodic and aperiodic trend respectively. More details are shown in the next section.

3. Simulation results and phenomena analysis

In practical applications, the monopulse radar needs to continuously observe the target to obtain the angle information. This section verifies the decoying effect of RCS modulated corner reflectors in the continuous angle tracking.

During the automatic tracking process, the antenna servo system updates the beam direction in real time according to the measurement result. As shown in Fig. 7, the radar inputs the current measured angle into the tracking filter to obtain the predicted value at the next moment, to which the equisignal axis will point in the next measurement cycle.

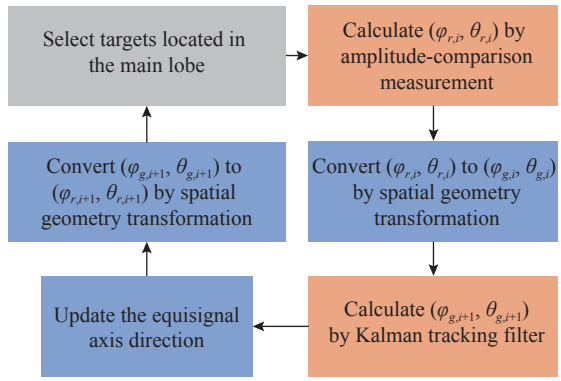

Fig. 7 Angle tracking process of the monopulse radar

The processes can be summarized as follows.

Step 1 Determine the scattering points located in the main lobe.

Step 2 Calculate angles $(\varphi_{r,i},\theta_{r,i})$ between the apparent angle and the equisignal axis at time i.

Step 3 Convert $(\varphi_{r,i},\theta_{r,i})$ to the global angles $(\varphi_{g,i},\theta_{g,i})$ through the spatial geometric transformation.

Step 4 Input $(\varphi_{g,i},\theta_{g,i})$ into the Kalman tracking filter to get the predicted value $(\varphi_{g,i+1},\theta_{g,i+1})$ at the next moment. The state vector is

$$\boldsymbol{X}(i)=\begin{bmatrix}x(i)\\ \dot{x}(i)\\ y(i)\\ \dot{y}(i)\\ z(i)\\ \dot{z}(i)\end{bmatrix}=\begin{bmatrix}\cos\theta_{g,i}\cos\varphi_{g,i}\\ \dfrac{\cos\theta_{g,i}\cos\varphi_{g,i}-\cos\theta_{g,i-1}\cos\varphi_{g,i-1}}{T}\\ \cos\theta_{g,i}\sin\varphi_{g,i}\\ \dfrac{\cos\theta_{g,i}\sin\varphi_{g,i}-\cos\theta_{g,i-1}\sin\varphi_{g,i-1}}{T}\\ \sin\theta_{g,i}\\ \dfrac{\sin\theta_{g,i}-\sin\theta_{g,i-1}}{T}\end{bmatrix} \tag{13}$$

where $x(i)$, $y(i)$, and $z(i)$ are the direction cosines with corresponding change speeds $\dot{x}(i)$, $\dot{y}(i)$, and $\dot{z}(i)$.

Step 5 Update the equisignal axis direction to $(\varphi_{g,i+1},\theta_{g,i+1})$ and repeat Step 1.

The simulation parameters are shown in Table 1.

Table 1 Simulation parameters

Parameter	Value
Initial target position/m	(8 000,4 000,8 000)
Target velocity/(m·s^{-1})	(−200,0,0)
Target RCS/m^2	2
Mainlobe width/(°)	2.72
Beam deviation angle/(°)	0.5
Bandwidth/MHz	0.5
Carrier frequency/GHz	11
Pulse width/μs	5
Signal-to-noise ratio/dB	20
Measuring sampling period/s	0.005
Tracking sampling period/s	0.005
Standard deviation of the system noise	0.1
Standard deviation of the observation	(0.02,0.01,0.02)

Suppose that there are four electronically controlled corner reflectors with a uniform interval of 50 m, decoying effects under different jamming implementations are simulated accordingly and evaluated by the maximum value and the range of the decoy ratio.

3.1 Synchronous change

The synchronous change means that time-domain RCS modulation signals of all corner reflectors are the same. Fig. 8 and Fig. 9 are the decoy ratios corresponding to the uniform intermittent and pseudo-random signals with different duty ratios respectively. It can be seen that decoy ratios of the four signals all fluctuate between 27% and 53% with the same extreme values, which shows that the signal form and duty ratio have little influence on the interference effect when the corner reflector is modulated synchronously. This is because that all corner reflectors are in the penetration or the reflection state at the same time since the modulation signals are exactly the same, the duty ratio only affects the duration of the extreme values.

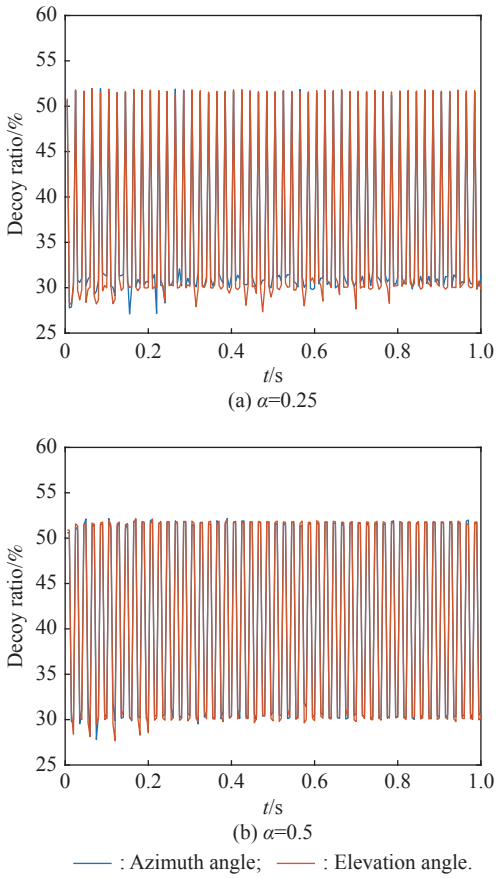

Fig. 8 Decoy ratios of the uniform intermittent signal with different duty ratios under the synchronous change pattern

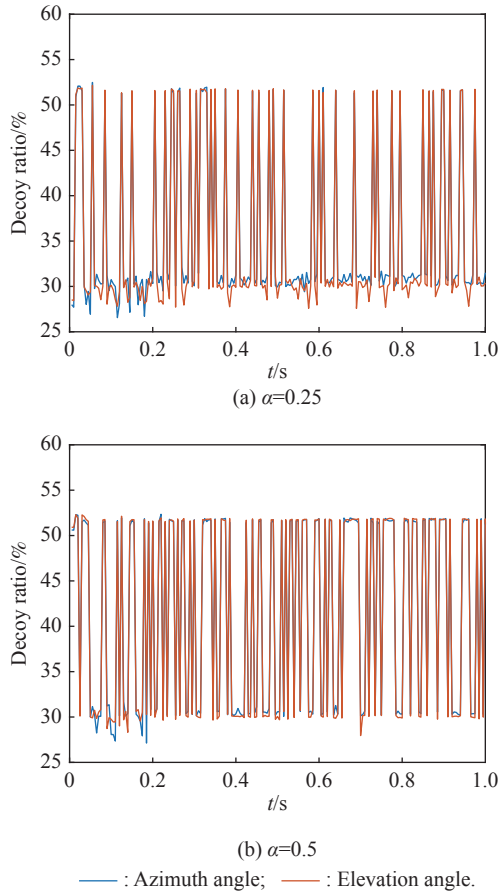

Fig. 9 Decoy ratios of the pseudo-random signal with different duty ratios under the synchronous change pattern

3.2 Cyclic shift

The cyclic shift means that the RCS modulation signal of the latter corner reflector lags behind the previous one by a code width:

$$\sigma_{i+1}(t) = \sigma_i(t) \otimes \delta(t - \tau_0). \tag{14}$$

It can be seen from Fig. 10 and Fig. 11 that the jamming effect of the cyclic shift is better than that of the synchronous modulation, and the decoy ratio range of the pseudo-random signal is larger than that of the uniform intermittent one when the duty ratio α is 0.25. This indicates that the interference effect in which all the corner reflectors are in the unified state at the same time will be reduced, which is consistent with the trend of the purple curve in Fig. 3. In addition, increasing α has no effect on the jamming effect in Fig. 11, but can slightly increase the measurement error of the uniform intermittent signal in Fig. 10.

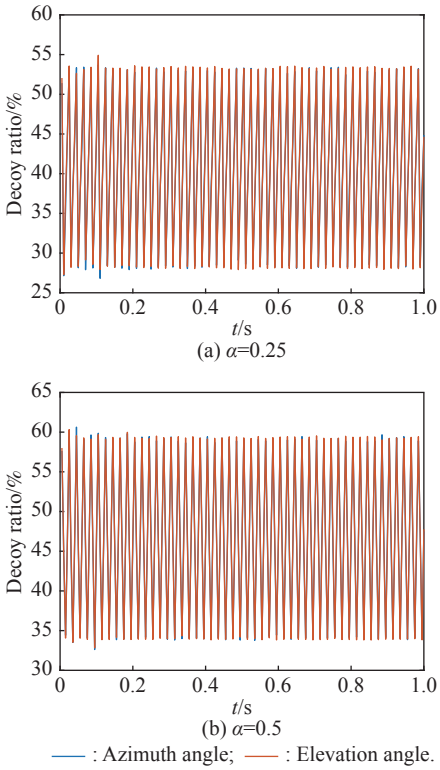

Fig. 10 Decoy ratios of the uniform intermittent signal with different duty ratios under the cyclic shift pattern

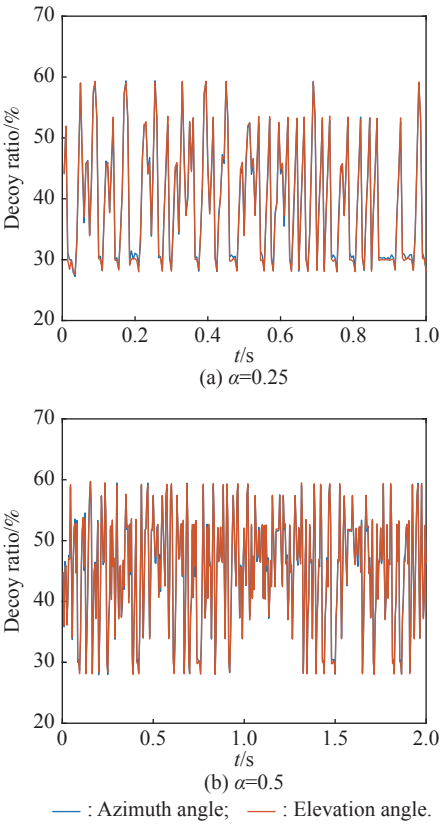

Fig. 11 Decoy ratios of the pseudo-random signal with different duty ratios under the cyclic shift pattern

3.3 Random change

Assuming that the RCSs of all corner reflectors are modulated by mutually independent pseudo-random signals, Fig. 12 shows a similar trend with Fig. 11, in which the distribution of the corner reflectors in different states are similar, and the maximum value and range of the decoy ratio can reach about 60% and 32% respectively.

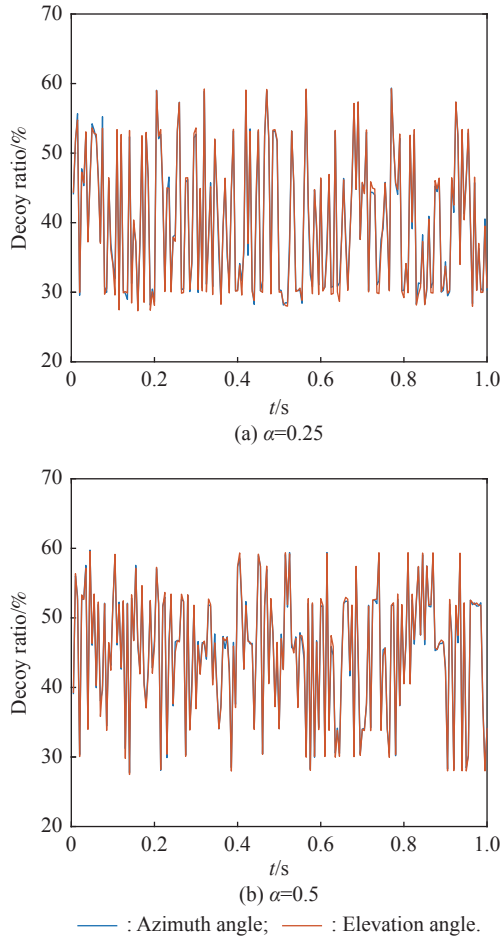

Fig. 12 Decoy ratios of the pseudo-random signal with different duty ratios under the random change pattern

Based on the above simulation results, the following conclusions can be drawn. First, the interference effect is essentially determined by the distribution of the corner reflectors in different states. Increasing the duty ratio can improve the jamming effect only in the case of uniform intermittent signal under the cyclic shift pattern due to the spatial distribution rearrangement of the corner reflectors. Second, the decoying effect will be reduced when the corner reflectors are all in a unified state, and could be better under modulations with the stronger non-periodicity.

4. Conclusions

In this paper, an angular blinking jamming method based on an electronically controlled corner reflector is proposed, which can achieve active interference effects by the passive means. Simulation results show that the apparent center can be deviated from the target with a continuous sharp flicker through the RCS modulation of corner reflectors, and the interference effect under the pseudo-random modulation is the best in comparison with other patterns.

References

[1] SHERMAN S M, BARTON D K. Monopulse principles and techniques. Norwood: Artech House, 2011.

[2] LEONOV A I, FOMICHEV K I. Monopulse radar. Norwood: Arctech House, 1986.

[3] ADAMY D. EW 101: a first course in electronic warfare. Norwood: Artech House, 2001.

[4] DU PLESSIS W P. A comprehensive investigation of retrodirective cross-eye jamming. Pretoria, South Africa: University of Pretoria, 2010.

[5] WANG J T, GENG X M, ZHANG D. Analysis on influence of synchronous blinking jamming to radar seeker antenna. Proc. of the 4th International Conference on Wireless Communications, Networking and Mobile Computing, 2008. DOI: 10.1109/WiCom.2008.547.

[6] LI P, GENG X M, ZHANG Y, et al. The analysis on angle noise produced by blinking jamming. Proc. of the International Asia Conference on Informatics in Control, Automation and Robotics, 2009: 441–444.

[7] KERINS W J. Analysis of towed decoys. IEEE Trans. on Aerospace and Electronic Systems, 1993, 29(4): 1222–1227.

[8] LIU T P, LIU Z, LIAO D P, et al. Platform skin return and multiple-element linear retrodirective cross-eye jamming. IEEE Trans. on Aerospace and Electronic Systems, 2016, 52(2): 821–835.

[9] LIU T P, LIAO D P, WEI X Z, et al. Performance analysis of multiple-element retrodirective cross-eye jamming based on linear array. IEEE Trans. on Aerospace and Electronic Systems, 2015, 51(3): 1867–1876.

[10] LIU S Y, DONG C X, XU J, et al. Analysis of rotating cross-eye jamming. IEEE Antennas and Wireless Propagation Letters, 2015, 14: 939–942.

[11] ACHOURI K, CALOZ C. Design, concepts, and applications of electromagnetic metasurfaces. Nanophotonics, 2018, 7(6): 1095–1116.

[12] CUI T J, LIU S, ZHANG L. Information metamaterials and metasurfaces. Journal of Materials Chemistry C, 2017, 5(15): 3644–3668.

[13] SO H, ANDO A, SEKI T, et al. Multiband sector antenna with the same beamwidth employing multiple woodpile metamaterial reflectors. IEICE Trans. on Electronics, 2014, 97(10): 976–985.

[14] DECENA B A, LUZON J R, PURISIMA M C L. 2.4 GHz pattern reconfigurable corner reflector antennas using frequency selective conductor loops and strips. Proc. of the IEEE Region 10 Conference, 2017: 2914–2919.

[15] TANIZAWA Y, CHO K, SO H, et al. Radiation characteristics of corner reflector antenna employing frequency selective surface. Proc. of the URSI Asia-Pacific Radio Science Conference, 2016. DOI: 10.1109/URSIAP-RASC.2016.7883533.

[16] CHATTERJEE A, PARUI S K J I T O A, PROPAGATION. Beamwidth control of omnidirectional antenna using conformal frequency selective surface of different curvatures. IEEE Trans. on Antennas and Propagation, 2018, 66(6): 3225−3230.

[17] CHATTERJEE A, PARUI S K. Performance enhancement of a dual-band monopole antenna by using a frequency-selective surface-based corner reflector. IEEE Trans. on Antennas and Propagation, 2016, 64(6): 2165–2171.

[18] ELZWAWI G H, KESAVAN A, ALWAHISHI R, et al. A new corner-reflector antenna with tunable gain based on active frequency selective surfaces. IEEE Open Journal of Antennas and Propagation, 2020, 1: 88–94.

[19] MAMEDES D F, NETO A G, BORNEMANN J. Reconfigurable corner reflector using PIN-diode-switched frequency selective surfaces. Proc. of the IEEE International Symposium on Antennas and Propagation and North American Radio Science Meeting, 2020: 127–128.

[20] NAJAFNEZHAD E, NOURINIA J, GHOBADI C, et al. A high gain dual-band printed antenna for LTE base stations with a corner reflector. AEU-International Journal of Electronics and Communications, 2018, 87: 173–179.

[21] ZHU J X, PEI Z B, QU S B, et al. A design of a new dihedral corner reflector loaded with meta-material absorbing layer. Journal of Air Force Engineering University, 2013, 14(6): 85–88. (in Chinese)

[22] ZHU J X, PEI Z B, QU S B, et al. Design of novel trihedral corner reflector loaded with meta-material absorbing body. Electronic Components and Materials, 2013, 32(10): 52–54.

[23] ZHANG Z K, WANG D H, LEI Y S, et al. A novel RCS enhancing device based on metamaterial. Radio Engineering, 2017, 47(5): 67–70.

[24] LEI X, ZOU Y T, SHANG Y P, et al. Backscattering enhancement of an obtuse dihedral corner structure through metasurface. Electronic Components and Materials, 2019, 38(8): 99–105.

[25] ZHANG R, FENG D J, XU L T. Design and polarization characteristics analysis of dihedral based on Salisbury screen. Journal of Radars, 2016, 5(6): 658–665. (in Chinese)

[26] DING L F, GENG F L. Radar principle. Xi'an: Xidian University Press, 2002. (in Chinese)

[27] GAN L, SUN G, FENG D, et al. Characteristics of an eight-quadrant corner reflector involving a reconfigurable active metasurface. Sensors, 2022, 22(13): 4715.

Biographies

GAN Lin was born in 1999. She received her B.E. degree in information engineering from the College of Electronic Science and Technology, National University of Defense Technology, Changsha, China, in 2016. She is pursuing her M.S. degree of information and communication engineering in the College of Electronic Science and Technology, National University of Defense Technology. Her research interest concentrates on radar passive jamming technology.

E-mail: ganlin16@nudt.edu.cn

WU Zehao was born in 1999. He received his B.E. degree in information countermeasures technology from the College of Electronic Engineering, National University of Defense Technology, Hefei, China, in 2021. He is pursuing his M.S. degree in electronic information at the College of Electronic Science and Technology, National University of Defense Technology. His research interest concentrates on radar passive jamming technology.
E-mail: wuzehao17@163.com

WANG Xuesong was born in 1972. He received his B.Sc. and Ph.D. degrees from the College of Electronic Science and Technology, National University of Defense Technology (NUDT), Changsha, China, in 1994 and 1999, respectively. He is currently a professor with NUDT and his research interests concentrate on radar information processing and target recognition. He is a fellow of the Chinese Institute of Electronics. His Ph.D. dissertation was awarded as one of the 100 excellent Ph.D. dissertations, China, in 2001 (two years after his graduation). He was also granted the National Science Fund for Distinguished Young Scholars and other similar talent titles.
E-mail: wxs1019@vip.sina.com

LI Jianbing was born in 1979. He received his B.E. and M.E. degrees in aerospace science from the College of Aerospace Science and Engineering, National University of Defense Technology (NUDT), Changsha, China, in 2002 and 2004, respectively, and Ph.D. degree in information and communication engineering for his work on the analysis of wake vortices' scattering characteristics from the College of Electronic Science and Engineering, NUDT, in December 2010. He is currently working as a full professor with the College of Electronic Science and Technology, NUDT. His research interests include new concept radar design and distributed soft target detection.
E-mail: jianbingli@nudt.edu.cn